Low Pressure Corium Dispersion Experiments with Lateral Failure in the Bottom Head of the Pressure Vessel

L. MEYER, M. GARGALLO

Forschungszentrum Karlsruhe, Institut für Kern-und Energietechnik,
Postfach 3640, 76021 Karlsruhe, Germany, e-mail: meyer@iket.fzk.de

ABSTRACT

Experiments were performed in a scaled annular cavity design, to investigate melt dispersal from the reactor pit when the reactor pressure vessel lower head fails at low system pressure of less than 2 MPa.

In the part of the experimental program presented in this paper, the fluid dynamics of the dispersion process was studied using model fluids, water or bismuth alloy instead of corium, and nitrogen or helium instead of steam. The effects of different breach sizes and locations, and different failure pressures on the dispersion were studied, specifically by testing central holes, lateral holes, horizontal rips, and complete ripping of the bottom head.

The experiments have shown, that lateral failures lead to smaller melt dispersal out of the reactor pit than failures in the central part of the lower head. With holes at the base of the bottom head, the most important parameters governing the dispersion of melt are the hole size and the burst pressure. The fraction dispersed into the reactor compartments increases with larger holes and higher pressures. Values up to 76% have been found for both melt simulant liquids, water and metal. With lateral breaches the liquid height in the lower head relative to the upper and lower edge of the breach is an additional parameter for the dispersion process, and usually not all the liquid is discharged out of the RPV. The liquid fraction entrained out of the RPV can be higher with a small breach than with a large one, because of the longer blowdown time. With lateral failures maximum dispersed fractions of 50% were found with water as melt simulant and less than 1% with liquid metal. The results from the liquid metal tests represent the lower bound for the dispersed melt fractions, however, they are probably closer to the expected values than the results from the water tests, that represent the upper bound. So, significantly less dispersion of melt can be expected for lateral breaches at pressures below 2 MPa, probably less than 10%. If higher dispersion occurs, due to higher pressure at failure or with failures near the bottom center, simple devices to mitigate the dispersion out of the cavity may be feasible.

1. INTRODUCTION

In a severe accident special pressure relief valves in the primary circuit of German Pressurized Water Reactors (PWR) and future European Reactors will reduce the system pressure below 2 MPa. However, a failure in the bottom head of the reactor pressure vessel, followed by melt expulsion and blowdown of the reactor cooling system, might disperse molten core debris out of the reactor pit, even at low pressures. The mechanisms of efficient debris-to-gas heat transfer, exothermic metal/oxygen reactions, and hydrogen combustion may cause a rapid increase in pressure and temperature in the reactor containment and are collectively referred to as Direct Containment Heating (DCH). Investigating the DCH-issue a number of problems have to be addressed: (i) final location of corium debris, (ii) loads on the containment in respect to pressure and temperature, (iii) amount of hydrogen produced, (iv) loads on reactor pit and support structures, (v) impact on safety components. Knowledge of these points can lead to realize additional safety margins for existing plants and is needed for the development of the next generation of nuclear power plants. Specifically, the final location of the corium debris determines the efficacy of the melt collecting and cooling concepts that are planned for future reactors.

Melt dispersal and DCH phenomena have been investigated intensively mainly for cavity designs with large instrument tunnels leading into the compartments, relatively high melt ejection pressures and small holes centered at the lower head [1]. However, only few works have studied these phenomena with an annular cavity design similar to that of some European PWRs and the European Pressurized Reactor (EPR), where the only large pathway out of the reactor pit is the narrow annular gap between the reactor pressure vessel (RPV) and the cavity wall. Moreover, there are few works which study RPV failures during low pressure melt ejection scenarios [2-5]. Therefore, our experimental program is aimed at low failure pressures, diverse failure modes and larger breach sizes using an annular cavity design similar to that of the planned EPR.

Our experimental program has three parts. The first part has been completed in 1998. This comprised two experiments performed at the Sandia National Laboratories (SNL) in cooperation with Forschungszentrum Karlsruhe (FZK), Institut de Protection et de Sûretè Nucléaire (IPSN) and the U.S. Nuclear Regulatory Commission (NRC) [4]. These tests were performed with thermite melt, steam and a prototypic atmosphere in the containment in a scale 1:10. The results showed that failures at low system pressures can lead to a considerable ejection of liquid out of the cavity. In the second part of the program a detailed investigation of geometry effects has been performed. The test facility DISCO-C (Dispersion of Simulated Corium) has been built at FZK for performing dispersion experiments with cold simulant materials in an EPR-typical geometry in a scale 1:18. In the third part of the program, selected experiments in a DISCO-H facility in the same scale will be performed with thermite melt, steam and a prototypic atmosphere in the containment. This paper reports on the results of the second part that is limited to fluid dynamic processes.

The experimental program is accompanied by analytical work with the objective to transform the experimental results to the prototypical case. Two fundamentally different methods are employed. One method is to correlate the experimental results regarding the dispersed fraction of melt with a single function of similarity numbers [6]. This function will then be applied to prototypical conditions. The other method makes use of codes to calculate the pressure and the melt dispersal [7]. The models used in the codes are validated by comparison with experimental results. With both methods an extrapolation out of the range of experimental parameters is necessary and a careful assessment of scaling is essential.

2. SCALING CONSIDERATIONS

Several different scaling analysises for severe accident modeling have been performed by different authors [8-10]. Based on the method of Tutu and Ginsberg [10], that starts with the differential equations describing the processes, a scaling analysis was performed for the isothermal DISCO experiments [6]. Common to all analysises is the necessity to neglect some processes. Thus, the mode of melt discharge was not considered, but it was assumed that after the discharge of the melt from the vessel, the melt spreads along the floor and the walls of the cavity as a liquid film. Thereafter, during gas blow-down, melt droplets are entrained from the film into the gas flow, neglecting droplet deposition, trapping and re-entrainment. A set of eleven dimensionless scaling groups were found and were evaluated for 54 DISCO cases in comparison with a reactor benchmark case. The DISCO cases included three different melt simulants, water, gallium alloy and Wood's metal, two driving gases, nitrogen and helium, and various different initial pressures and holes sizes. As expected, large mismatches of the groups between model and prototype could be observed. The cases with water as melt simulant showed the largest deviations, and certainly give to high values for the carry-over of dispersed melt from the cavity. Certain cases with Wood's metal seemed to give a lower bound for the dispersed melt fraction.

The main conclusion from all scaling considerations is that an exact geometrical scaling is essential. If the volumes of gas and liquid are scaled accordingly (length scale to the power of 3), the initial pressure can be scaled 1:1. Then the gas velocity and the droplet size are mainly functions of the properties of the model fluids used. The duration of the blow down is scaled as the length scale. Central for similarity is the ratio of characteristic times, e.g. the ratio of the dispersal time to the time constant of the blowdown, defined as the coherence ratio [11]. Again, if the geometry including the failure mode is modeled accurately, this parameter depends mainly on the properties of the model fluids used.

We know that all scaling methods are flawed because of the negligence of certain flow processes and the large uncertainty in the scale-up capability of available entrainment correlations. However, if all relevant experimental results can be recalculated either by codes or by similarity correlations we can have confidence in extrapolating to the reactor case with the same tools.

3. TEST FACILITY

3.1 Experimental set up

A scheme of the experimental set up is shown in Fig. 1. In Fig. 2 more details are shown, including the positions of the pressure (P) and temperature (T) measurements. The model matches the EPR-geometry in a scale 1:18. The main components of the test facility are:

1.   The pressure vessel consists of a steel pipe with a model of the reactor pressure vessel (outer diameter 298.5 mm) at its lower end. It has a total volume of 0.0879 m³, that models the volume of the EPR pressure vessel and the volume of part of the RCS. A disk holding 8 pipes (44 mm I.D. 250 mm length), which model the flow constriction through the main cooling lines, separates the two partial volumes in a ratio 60:40 (RCS:RPV). The lower head of the RPV can hold $3.4 \cdot 10^{-3}$ m³ of liquid, which corresponds to 20 m³ or 160 t of corium.

2.   The cavity, a Plexiglas cylinder with an inner diameter of 342 mm, is attached to the vessel support structure. The main flow path out of the cavity is the annular gap between the inner wall of the reactor pit and the RPV. This annular gap, with a total flow cross section of 0.02188 m², leads to the main coolant lines and subsequently to the compartments. The way straight up into the containment does not exist. There is a second possible flow path out of the cavity through four ventilation openings in the lower part of the Plexiglas cylinder, which lead to the melt spreading room. However these openings were closed in all of the experiments except in one special test.
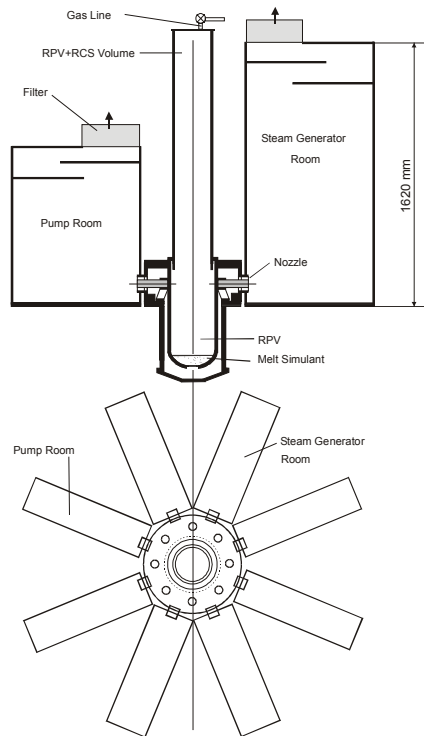
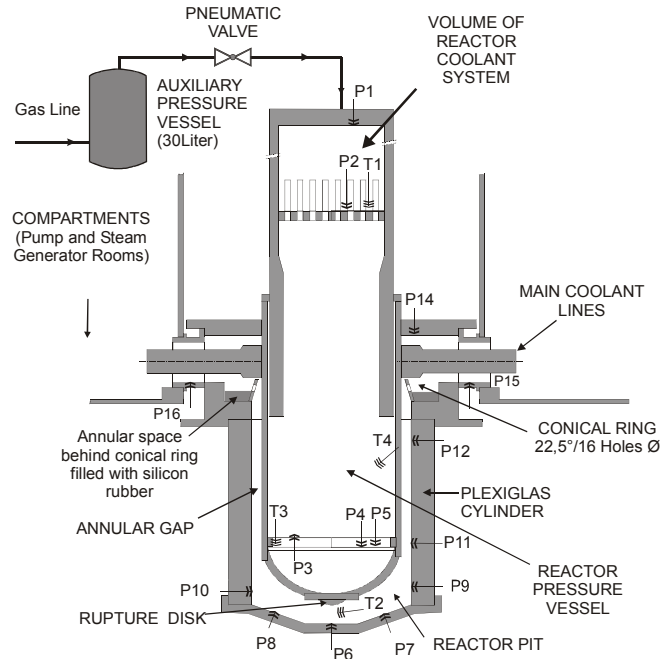**Fig.1.** Test facility configuration

Fig. 2. Pressure vessel, cavity and instrumentation

3. The eight <u>main coolant lines</u> are modeled each one by a rod inside a pipe. These annular nozzles have a total flow cross section of 0.03077 m².

4. The <u>compartments</u>, eight boxes which model in volume the steam generator and pump rooms (0.3 m³ and 0.131 m³ each respectively), are connected to the nozzles and are placed on the vessel support structure around the RPV. They are covered by filters on their tops for the extraction of fog and drops. Two boxes have one Plexiglas wall to permit optical access for flow visualization.

5. A conical ring at the <u>pressure vessel support</u>, that represents a constriction for the flow, with 16 holes with a diameter of 26 mm. The total flow cross section through the vessel support reduces then to 0.01890 m². There is a space behind this conical ring, where liquid can be collected during the experiments. To reduce the trapping of liquid, the space was filled with silicon rubber up to the height of the 16 holes in some of the latter experiments.

3.2 Failure modes

The following failure modes of the lower head were studied: central holes and three types of lateral breaches, lateral holes, horizontal slots, and complete ripping and tilting of the lower head.

The central holes positioned at the bottom of the RPV were closed by a rupture disk with an opening diameter somewhat larger then that of the hole (Fig.3.a). A similar construction was employed for round holes of 25 and 50 mm diameter on the side of the lower head (Fig.3.c and d). The inclination of the axis of the holes is 45 degrees. Their center measured at the inside is 50 mm above the bottom of the calotte. So, the lower edges of the holes at the inside are 41.15 and 32.4 mm above the bottom of the calotte, respectively. A horizontal slot, that models a partial rip in the lower head, as it might occur with a side-peaked heat flux distribution, was also placed in a 45 degrees axis but with the lower edge 56.1 mm above the bottom of the calotte (Fig.3.b). The slot is 12.5 mm wide (high, inclined 45 degrees), and 42.5 mm long with a 6.25 mm radius. The flow cross section is equivalent to a 25 mm hole. The third type of lateral breaches models the horizontal rip propagating around the circumference of the lower head leaving

only a small section attached (Fig.3.e), as it was observed in the lower head failure (LHF) experiments performed at SNL [12]. Here the calotte is a separate part that is held in position by a steel rod from below at its center. When it is released the lower head moves down on one side and is held by a hinge on the opposite side. It is stopped by crushing material on four pedestals. Two different heights of pedestals were used to obtain different flow cross sections. The drop height was h = 56 mm in two tests, and h = 16 mm in two other tests. The drop height at the side of the hinge was not zero but varied between 0.5 mm and 2 mm. The total flow cross section was 220 cm² and 70 cm², respectively. For comparison, the cross section of a 100-mm-hole is 79 cm² and for a 50-mm-hole it is 20 cm².
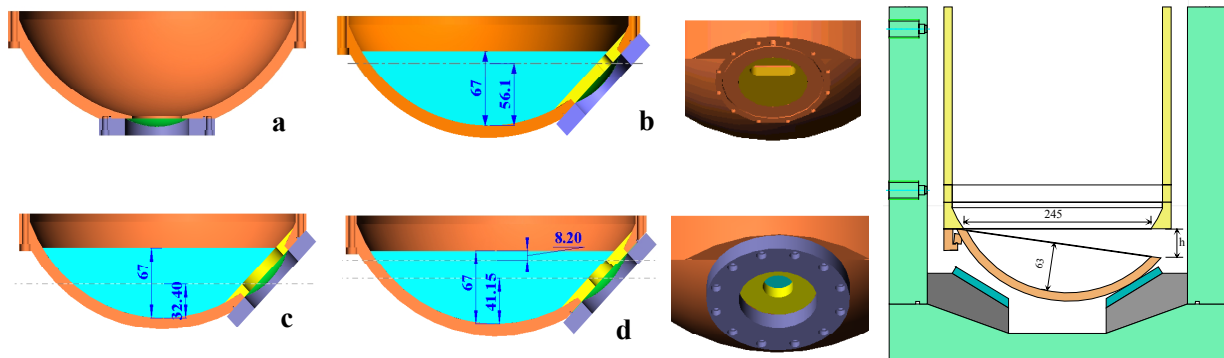
Fig. 3 Failure geometries used in DISCO-C

a. Central hole   b. Lateral slot, equivalent to ⌀25mm   e. Unzipping and tilting of
c. Lateral hole, ⌀50 mm   d. Lateral hole, ⌀25 mm   the lower head

3.3 Geometry variations

To investigate the effect of different initial liquid pool depths a standpipe was mounted inside the pressure vessel (Fig. 4). The standpipe can hold the same amount of liquid as the lower head. A similar geometry was also used by Bertodano et al. [2] and Kim et al. [5]. To test the effect of the venting openings in the reactor pit, a cavity model was used with four holes in the lower part of the pit that were connected by a circumferential channel and a tube leading to an extra compartment that models the spreading room (Fig. 5). The four holes had a total flow cross section of approximately ¼ of the minimum flow cross section below the RPV support girder, and with the diameter of 38 mm they took up 14% of the circumference of the pit. In another modification of the cavity the diameter of the cavity was changed from 342 mm to 386 mm, increasing the width of the annular gap from 21.75 mm to 43.75 mm. The minimum flow cross section below the nozzles was kept constant. In the wider cavity an extra cylinder was inserted, that should trap the liquid mass and prevent the dispersion out of the cavity (Fig.6).
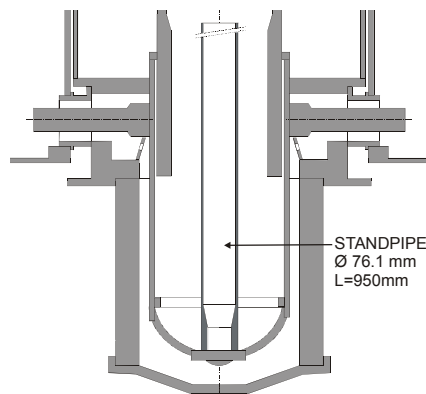

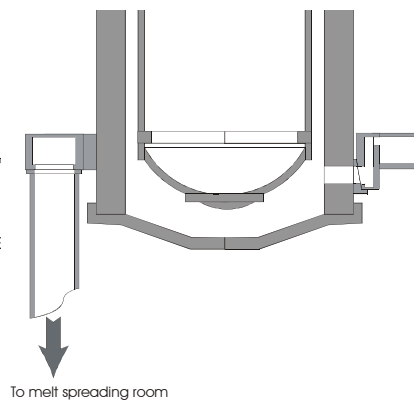**Fig. 4.** Standpipe to model high pool depth

Fig. 5. Cavity with openings leading into the melt spreading room
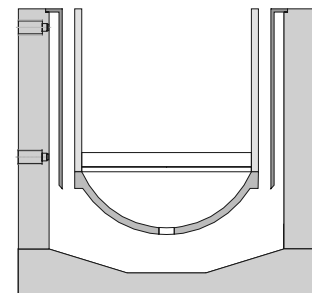
Fig. 6. Melt trapping device in the cavity

4. EXPERIMENTAL PROCEDURE

The fluids employed in this test series were water or a bismuth alloy (MCP-58®, similar to Wood's metal) instead of corium, and nitrogen or helium instead of steam. Most experiments were performed for the combination water/nitrogen, with 3.4×10^{-3} m³ of water. With central holes four hole sizes, 15, 25, 50 and 100 mm diameter, were investigated, each at three initial pressures, 0.35, 0.6 and 1.1 MPa. With helium all four hole sizes were tested, but only at 0.65 MPa. Only the 25-mm-hole was tested at all three pressures. Nitrogen/metal tests were performed with the 25 and the 50-mm-hole at 0.6 and 1.1 MPa with 3.3×10^{-3} m³ of metal. Some tests (25 and 50 mm hole size) were performed with 1.8×10^{-3} m³ of water and were repeated several times. The reproducibility was very good. The parameters of the tests with lateral breaches and geometry variations are given in the respective sections.

Table 1. Properties of model fluids

Property		Helium	Nitrogen	Water	Bismut-alloy Bi 49.5, Pb 17.6 Sn 11.6, In 21.3
Molecular weight	kg/kmol	4.003	28.013	18.015	165
Gas constant	J/kg K	2077.22	296.8	-	-
Density ρ at 10^5 Pa, 293 K	kg/m³	0.164	1.145	1000	9104
Dyn.Viscosity η at 293 K	10^{-3} Pa s	0.0196	0.0178	1.002	1.6 [1]
Surface tension σ	10^{-3} N/m	-	-	72	350 [1]

In the tests employing rupture disks, the pressure vessel is filled with gas to a pressure slightly lower than the failure pressure of the rupture disk. A small auxiliary pressure vessel (30 liter), filled to a somewhat higher pressure is connected to the main pressure vessel. By opening a valve electro-pneumatically in the line between the two vessels the pressure in the main vessel increases up to the failing pressure of the rupture disk and the blowdown starts. A break wire at the hole gives the signal for closing the valve again and for the time mark t = 0. The valve is fully closed at t = 70 ms. In the tests with the declining lower head the experiment was started by breaking the bolts that held the rod in place by detonators.

Transient pressures were measured at 30 positions in the vessel, the cavity and the compartments. Piezo-resistive transducers were used, (Kistler, RES12A), with ranges 0.2, 0.5, 1.0 and 2.0 MPa absolute pressure. The sensors are compensated in the temperature range –20..+120°C. The sensors have a diameter of 12 mm and are mounted in the wall with the steel diaphragm almost flush with the wall. They have a high natural frequency, good linearity, low hysteresis (±0.3% FSO) and good reproducibility (<0.2%).

Although the DISCO-C experiments are not intended to investigate thermal effects, temperatures must be measured because the gas temperature changes during the blowdown and the liquid metal must be heated above the melting temperature of 58°C. Three thermocouples in the pressure vessel and one in the lower cavity measured the gas and liquid temperature. The K-type thermocouples have a diameter of 0.36 mm. The time constant τ for gas temperature measurement is between 0.5 s and several seconds, depending on the heat transfer coefficient, with an estimate for our conditions of 0.6 s $< \tau <$ 1.2 s. Therefore all temperature signals for gas will be attenuated.

With the information of pressure and temperature in the pressure vessel and in the cavity, and the flow cross section of the annular space around the RPV, a mean gas velocity in the annular gap, u_G, can be determined. In order to determine velocity profiles across the gap, the Particle Image Velocimetry (PIV)

---

[1] estimated for T = 80°C by taking the properties of the components from Liquid-Metals Handbook, NAVEXOS P-733, Atomic Energy Commision, Washington, D.C. 1952

technique was applied in two tests. The measurement position was at the level of the pressure transducer No. 12 (P12 in Fig.2). Also the velocities of the droplets and the liquid jets were determined by PIV behind the nozzle at the entrance to a compartment in a few water tests. Drop sizes could also be established by the digital images taken during the PIV measurements. However, droplets smaller than 220 μm could not be found due to the limitation by the pixel size.

The mass fraction of the water or liquid metal in the compartments was determined by weighing the boxes before and after the test with a precision scale with an uncertainty of ±0.1 gram. The water in the cavity was absorbed in dry cloth, that was weighed. The metal was solid after the test and could be weighed directly.

Two high speed film cameras (LOCAM II, 500 frames/second) were used to record the flow phenomena in the cavity; they were arranged in a view angle of 90 degree to each other. Additionally two CCD-video cameras took pictures from the cavity for a quick view. The liquid flow into the compartments was filmed by a CCD-video camera with high shutter speeds (50 frames /second).

The pressure and temperature data were acquired by a Data Translation Board DT2839 at a sampling rate of 2.5 kHz. 30 channels for pressure and 4 channels for temperature were used. Additionally, signals were recorded from the electro-pneumatic valve (open/closed) and the break wire as a time-zero and sync-signal.

5. RESULTS AND DISCUSSION

5.1. Flow characteristics with central holes

5.1.1. Standard tests

The static pressure in the RPV and the total pressure on the cavity floor below the hole are shown for one typical test in Fig. 7. From the total pressure signal we can infer that there are four distinct stages of the outflow:

> 1. the single-phase liquid flow,
> 2. the blowthrough with two-phase flow,
> 3. single-phase choked flow, and
> 4. subsonic single-phase gas flow.

The duration of the individual stages depends on the hole size, the height of the liquid in the lower head, the pressure and the liquid density. The time of blowthrough can be expressed in terms of the height of the liquid at which the blowthrough occurs as function of the Froude number [13,15,16]. The time is short for large hole sizes d_h and high liquid velocities, i.e. high pressures and low liquid densities.
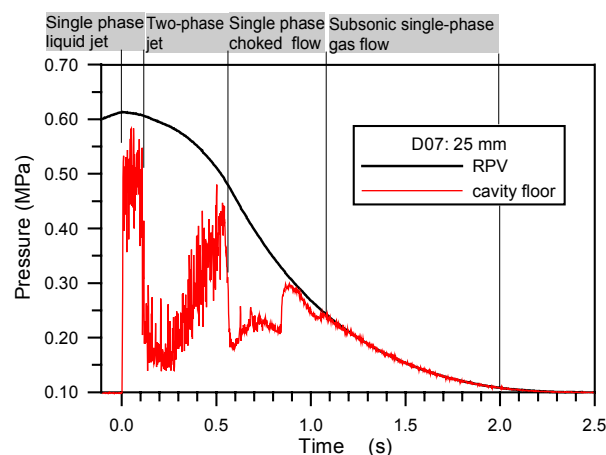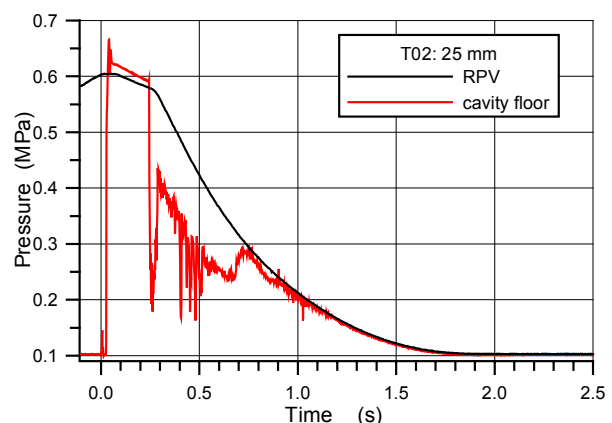

Fig.7. Pressure of test with central hole

Fig. 8. Pressure of test with liquid in standpipe

Single-phase liquid flow   Two-phase flow   Single-phase gas flow
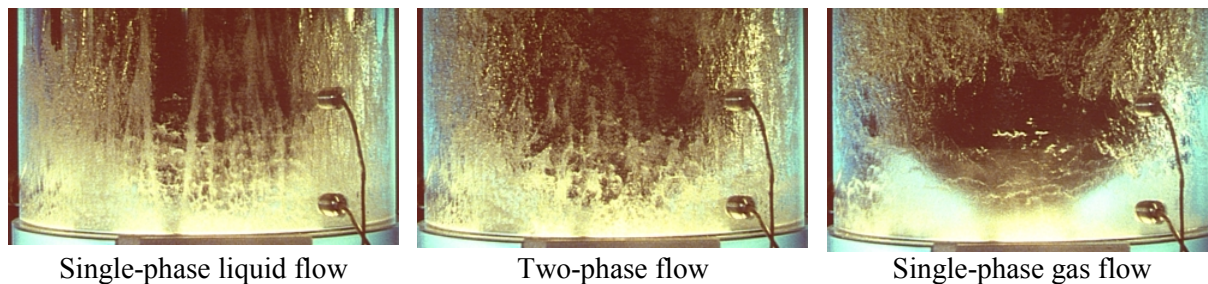
Fig. 9. Flow patterns in the cavity in a test with a central hole and water during different stages of the flow at the hole (25 mm dia., 0.35 MPa)
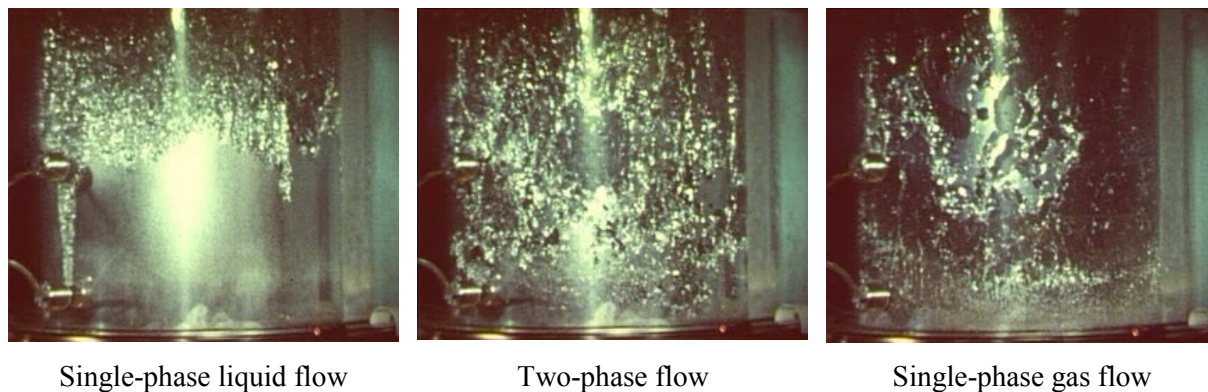

Single-phase liquid flow   Two-phase flow   Single-phase gas flow

Fig.10. Flow patterns in the cavity in a test with a central hole and liquid metal during different stages of the flow at the hole (50 mm dia., 0.6 MPa)

In the first stage, the single-phase liquid flow is driven by the static pressure in the vessel with the liquid velocity $u_L = (2 \, \Delta p \, / \, \rho_L)^{1/2}$. The exit velocities lie between 22 and 46 m/s for water, and between 10 and 14 m/s for liquid metal. The liquid moves up the cavity walls by its inertia and can reach the subcompartments before any gas has left the vessel (Fig. 9 and 10). During the second stage, the two-phase flow, the liquid is accelerated by the gas, within the jet as a dispersed droplet flow and in the cavity by shear force along the liquid film. This stage is important in the reactor case, because the thermal and chemical interaction between steam and melt is high due to the large liquid surface area. Liquid is easily carried out of the pit during this stage especially near its end when the velocity is high. The third stage is characterized by high gas velocities in the reactor pit, and if the mass flow rate of the gas is high enough large fractions of the liquid will be carried into the compartments. The bulk gas velocity in the annular gap determined by calculation from pressure and temperature data and by PIV-measurement agreed very well. Typical velocity profiles are shown in Fig.11 for a sample test. This test was a pure gas blowdown without any liquid. As expected, the flow was not developed and had a velocity maximum shifted to the RPV wall.
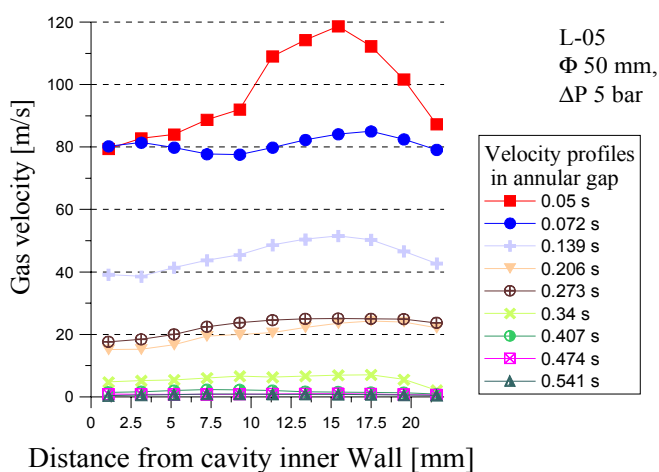
Fig. 11. Velocity profiles in the annular gap of the cavity (50 mm hole, 0.5 MPa)

a. liquid stream   b. droplet flow   c. droplet flow

Fig.12. Liquid flow at the nozzles (a and b: liquid metal, 50 mm hole, 0.6 MPa, c: water, 100 mm hole, 3.5 MPa)

By the video pictures taken from the compartments near the nozzles the liquid flow could be characterized qualitatively. In a few experiments (25 mm central hole, 0.6 and 1.1 MPa pressure, standard and standpipe tests with water and nitrogen) the velocity and size distribution of the droplets was determined quantitatively by PIV and image processing. Generally two different liquid flow structures occur. In one extreme the liquid flows in a stream through the nozzle into the compartments (Fig.12). On the other end there is a dispersed droplet flow. In most cases these two flow types occur in one test at different times, but mixed flow forms also occur (Fig.13). The parameters determining the flow type are the hole size, the pressure and the type of liquid used (table 2). With small hole sizes and low pressures liquid enters the compartments only as a stream. With any of the two parameters increasing, the gas velocity increases as well and generates a droplet flow. This starts usually near the end of the two-phase outflow, when the velocity reaches its maximum. The higher the gas velocity in the tests becomes, the smaller are the droplets. At the end of the blowdown liquid flows into the compartments as a rivulet again. With the largest holes or high pressure there is only the dispersed flow during the whole blowdown. With metal as liquid, the droplets are larger compared to water tests with the same hole size and same initial pressure.

Fig. 13. Water flow at nozzle (25 mm hole, 1.1 MPa)

Table 2. Test matrix of experiments with central holes. Shading denotes the flow structures occurring at the nozzles: ▤ liquid stream, ▨ droplet flow.

Hole ⌀ [mm]	Nitrogen /Water Pressure Δp [MPa]			Helium / Water Pressure Δp [MPa]			Nitrogen / Metal Pressure Δp [MPa]		
	0.25	0.5	1.0	0.25	0.5	1.0	0.25	0.5	1.0
15	stream	stream	stream/droplet		stream				
25	stream	stream/droplet	droplet	stream	droplet	droplet/stream		stream/droplet/stream	stream
50	droplet/stream	droplet	droplet				stream	stream/droplet/stream	stream
100	droplet	droplet	droplet						

| Drop velocities | Drop size distribution | Mass fraction per drop size |

Fig. 14. Parameters of droplet flow behind the nozzle at t = 677 ms, during single phase gas blowdown (25 mm hole, 0.6 MPa, water/nitrogen)

The quantitative picture is difficult to demonstrate, because the number, size and velocity of the droplets or liquid volumes entering the compartments varies in time and position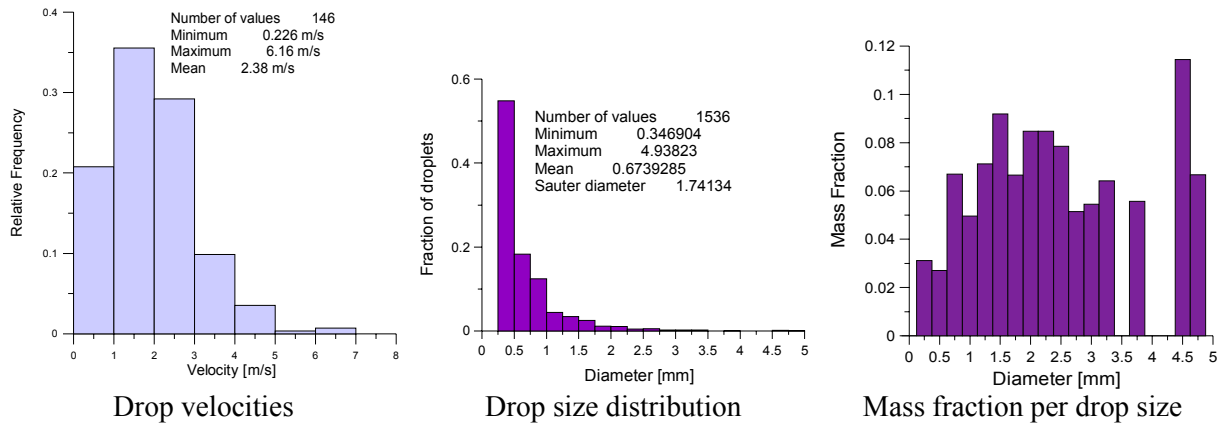. Thus, either mean data as function of time or histograms at specific times can be presented. For comparison with code results the history of representative droplet sizes, that is the Sauter diameter, together with their velocity and number (liquid fraction) at different positions (computational cells) would be useful. Here we can give only an impression of the large range of variation (Fig. 14). The largest number of drops is in the smallest drop size bracket but the main mass is carried by the larger drops (note, that droplets smaller 220 μm could not be registered). More data can be found in Ref. 16.

5.1.2 Effect of pool depth with central holes

With liquid contained initially in a standpipe, we get only three distinct stages of blow down, first the liquid jet and than the gas jet, initially as choked flow than as subsonic flow, practically without a stage of a two-phase jet in between. In these experiments the single-phase liquid outflow takes longer as in experiments with standard geometry, where the same liquid volume, failure pressure and hole dimensions were employed (Fig.8) . For example, in test D-07 the duration of this stage was approximately 106 ms (blowthrough time), while in test T-02 this stage takes 245 ms. The total duration of the blow down, however, is about 20% shorter for the tests with the water in the standpipe, because without the two-phase stage, the gas can leave the vessel earlier with higher velocity (Fig. 15).
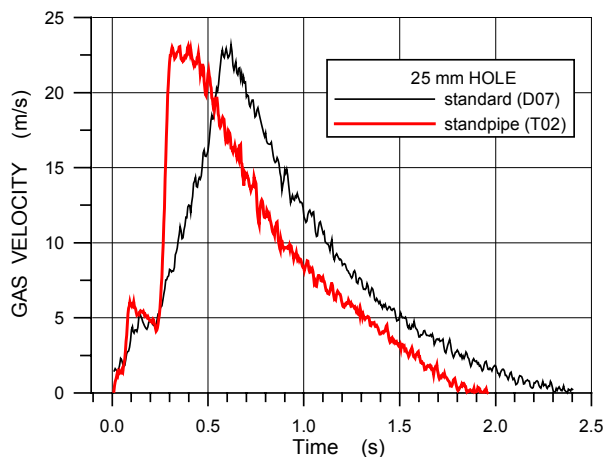

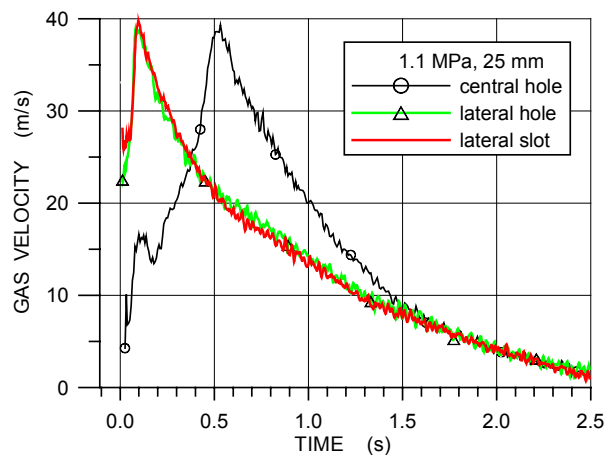**Fig. 15.** Bulk gas velocity in the annular gap of the cavity

Fig.16. Gas velocity in the cavity, comparison of different positions and shape of breaches
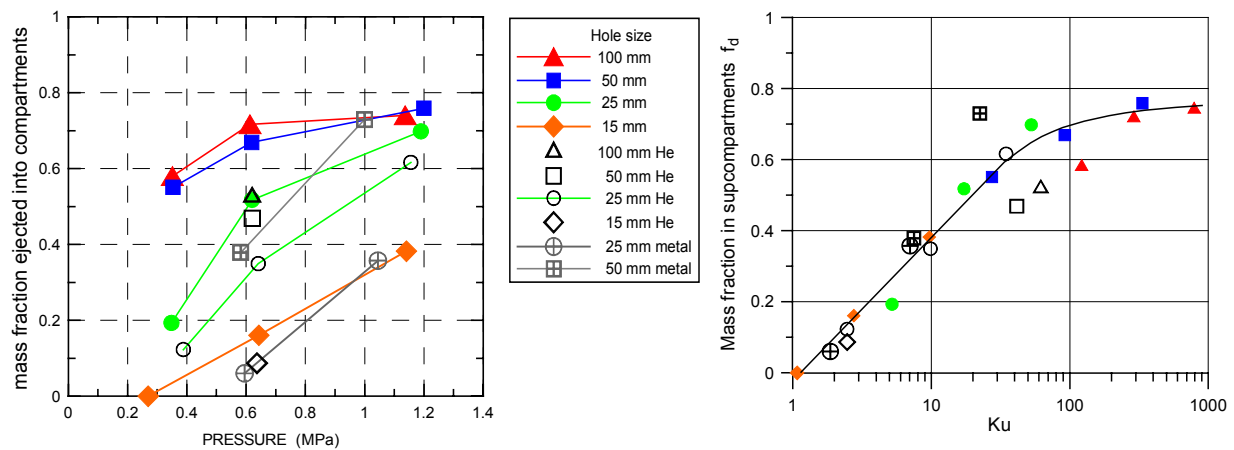
Fig. 17. Mass fraction ejected into compartments as function of the burst pressure and as function of the Kutadeladse number, for tests with central holes, and water/nitrogen (color), water/helium (open symbols) and liquid metal/nitrogen.

5.2. Dispersed fractions of liquid with central holes

Standard tests: The results of all standard tests with central holes are shown in figure 17. Liquid fractions larger than 0.76 were not found in the compartments, but this is a specific feature of the geometry. Up to 25% of the liquid were captured in the space at the support structure.

The results concerning the dispersed fractions into the compartments, f_d, could be correlated by the Kutateladze number[2] $Ku = \rho_G u_G^2 /(\rho_L g \sigma)^{1/2}$, with u_G, the maximum gas velocity in the annular space around the RPV, for all hole sizes, both driving gases, nitrogen and helium, and both liquids, water and Bi-alloy, with $f_d = 0.4 \log_{10}(Ku) \le 0.76$.

Effect of pool depth: In the tests with the water initially in the standpipe the dispersed liquid fractions are higher for both hole sizes, about 12% for the 50-mm-hole and 8% for the 25-mm-hole. Code calculations have produced similar results.

Effect of liquid mass: Most test with central holes were performed with 3.4×10^{-3} m^3 of water or 2.1×10^{-3} m^3 of Bi-alloy. The effect of different masses was investigated for the nitrogen/water combination with 25-mm-holes at two pressures, 0.6 and 1.1 MPa. The water mass was reduced from 3400 cm³ to 1800 cm³. The amount of mass trapped at the RPV support was about the same independent of the total mass. The mass fractions ejected into the compartments were reduced, from 70% to 55% in the 1.1 MPa tests, and from 52% to 41% in the 0.6 MPa tests. The ratio of the total masses was $r_{mt} = 1.89$ (3400/1800) and the ratio of the masses dispersed into the compartments was $r_{md} = 2.4$ for both pressures. This fact enables us to interpolate the dispersed melt fractions for intermediate values of pressures and masses.

Venting channel: One test with a initial pressure of 1.1 MPa and a central hole of 25 mm diameter was performed. No liquid was found in the melt spreading room and only 1.3 % of the liquid was in the circumferential venting channel after the test. Thus, the venting channel is not a preferred flow path for the melt, and the danger is low that large amounts of melt will reach the melt spreading room prematurely.

Wider cavity: Comparison with standard tests showed that the mass fraction ejected into the compartments was reduced from 70% to 63% (25 mm hole, 1.1 MPa). The maximum average gas velocity changed from 38 m/s to 17 m/s.

---

[2] The Kutateladze number represents the conditions to levitate droplets against gravity; some authors use Ku² for the same expression. Index G stands for gas and L for liquid.

Melt trapping device: In these tests it could be observed, that the cylinder separates the liquid at the cavity wall from the gas. The gas can flow into the compartments, while the liquid is trapped between the cylinder and the cavity wall. However, the liquid falls back into the lower cavity as soon as the top of the gap is reached and can be entrained by the gas, but at lower gas velocities. This reduces the dispersion substantially. With central holes of 25 or 50 mm diameter (1.1 MPa burst pressure) the reduction was from 63 % or 77%, respectively, with a wider cavity without trap, to 28 % with trap for both cases. With a lateral hole of 25 mm diameter (1.1 MPa) the reduction was from 36% to 10%.

5.3. Lateral breaches

All experiments with lateral breaches were performed with nitrogen as driving gas. Both, water and Bi-alloy were used as melt model fluids.

5.3.1. Lateral holes

Two experiments with burst pressures of 1.10 MPa were performed with holes of 25 mm (scaled 0.45 m) and 50 mm (0.90 m) diameter. Figure 18 shows the pressure in the pressure vessel. In these experiments we do not have the pressure signal from a transducer directly in front of the hole as an indicator of the different phases of the blowdown, especially for the determination of the blowthrough time. From the vessel pressure curve and the gas velocity curves (Fig.19 and 16) we can deduce that the blowthrough occurs very early (approximately at t ≤ 0.1 s). In Fig.18 we see that the theoretical pressure curves for single-phase gas flow are steeper than the measured one for test with the lateral hole (R04) at early times. Therefore, we can assume that the flow through the hole is two-phase at least up to t = 0.3 s. The liquid is carried out by entrainment of droplets from the pool surface inside the lower head, and the gas velocity is reduced.
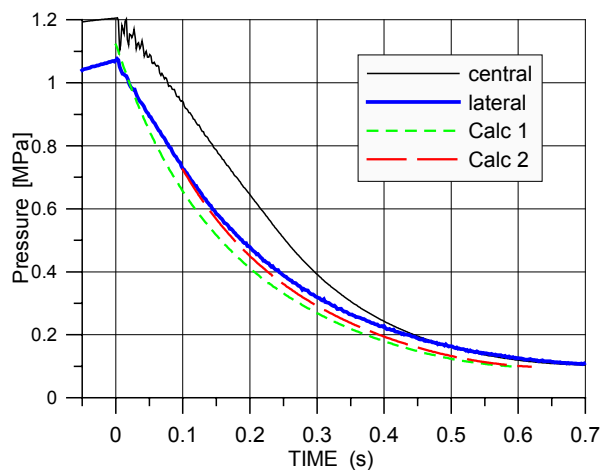
Fig. 18. Comparison of blowdown pressure of experiments with central hole and lateral hole, and with single-phase gas blowdown calculated for isentropic flow
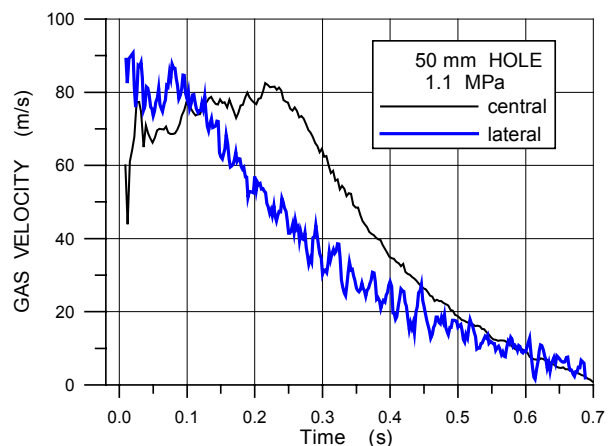
Fig. 19. Bulk gas velocities in the annular space in the cavity for tests with 50 mm-holes and liquid water, comparison of different hole positions

Fig. 20 shows pictures of the flow in the cavity. The main direction of the flow is not vertical as with central holes but in an angle of approximately 25 degrees, except near the breach, where the jet hits the side wall and spreads in all directions.

The ejected liquid was found mainly in the compartments opposite to the position of the hole. Not all of the liquid was ejected out of the RPV. The main parameter determining the fraction that remains in the lower head is, of course, the vertical position of the lower edge of the hole. It is, however, inter-

esting to see how much lower than this edge the water level is after the test. This number is a measure for the magnitude of the entrainment. Table 3 lists the data for the lower edge, the liquid level and the difference between the two in terms of a volume fraction (f_{entr}), that is equivalent to the fraction of liquid swept out of the lower head by entrainment. Although there is less water left in the calotte in test R04 with the larger hole than in R03 with the small hole, the entrainment was somewhat smaller in R04. There are two effects reducing the entrainment. With the large hole the blowdown time is shorter, and because the water level is already lower the surface area is smaller. With the high density liquid metal the entrainment in test R05 and R07 is much smaller than with water.
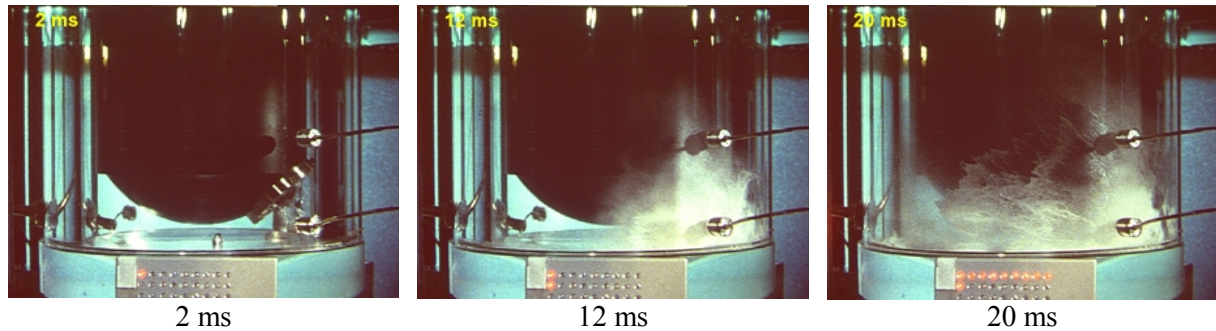

| 2 ms | 12 ms | 20 ms |

Fig. 20. Flow in the reactor pit in test with lateral slot, typical for all slots and holes

Table 3. Lateral breaks data on post test liquid level in the lower head and reduced dispersed fraction f_d* (pre-test level was 67 mm for the R-tests and 73 mm for K-tests)

Test	diameter or drop height [mm]	Liquid volume [10^{-3} m^3]	Burst pressure [MPa]	lower edge [mm]	water level [mm]	Diff. [mm]	f_{entr}	f_{RPV}	f_d	f_d*
R-01	slot, 25 equiv.	1.8 water	0.6	56	39	17	0.355	0.363	0.029	0.045
R-02	slot, 25 equiv.	1.8 water	1.1	56	33	23	0.455	0.262	0.250	0.339
R-03	hole, 25	1.8 water	1.1	41	21	20	0.290	0.111	0.358	0.403
R-06	hole, 25	1.8 water	1.6	41	18	23	0.315	0.085	0.469	0.513
R-04	hole, 50	1.8 water	1.1	32	14	18	0.200	0.048	0.477	0.501
R-05	hole, 25	1.8 metal	1.1	41	39	2	0.036	0.336	0.0005	0.0008
R-07	hole, 25	1.8 metal	1.6	41	38	3	0.054	0.296	0.0034	0.0048
K-01	drop height 56	2.1 water	0.5	-	-	15	0.174	0.095	0.011	0.012
K-04	drop height 56	2.1 water	0.8	-	-	18	0.202	0.067	0.091	0.098
K-02	drop height 16	2.1 water	0.8	-	-	25	0.401	0.187	0.225	0.277
K-03	drop height 16	2.1 metal	1.1	-	-	12	0.215	0.413	0.008	0.013

f = mass found post test in specific locations / total mass
f_d* = mass found post test in the compartments / (total mass – mass remaining in the RPV)
f_{entr} = volume in lower head between lower edge of hole and post test water level / total liquid volume

The fractions ejected into the compartments are smaller than in the experiments with central holes. Due to the smaller total mass (1800 cm³ versus 3400 cm³) we could expect a somewhat lower dispersed mass fraction, but the differences between corresponding tests with central holes and lateral holes are larger than what we have found as an mass effect. For 25-mm holes the mass effect is approximately 20 %, i.e. the dispersed fractions f_d with 1800 cm³ were only 80% of those with 3400 cm³.

Even if the dispersed fraction is determined in relation to the mass that was ejected out of the RPV, the difference is still large (f_d* in table 2, f_d* = f_d/(1-f_{RPV})).

Thus, for the 25-mm-hole and 1.1 MPa burst pressure we get the following effect on f_d:

Reducing the total mass from 3400 to 1800: f_d is reduced from 0.70 to 0.56
Moving the hole from central to the side : f_d is reduced from 0.56 to 0.36
f_d based on the mass ejected out of the RPV: f_d* is 0.40

For the 50-mm-hole we have a similar reduction (Fig. 21, 1.1 MPa); from f_d = 0.76 for a large total mass and central hole, to f_d* = 0.50 for the reduced dispersed fraction with smaller mass and lateral hole (R04). With higher pressure (1.6 MPa in test R06) the dispersed fraction increases also for lateral holes.

In the liquid metal test with a central hole the metal mass fraction ejected into the compartments was 36%, and 21% was captured at the RPV support. With the lateral hole practically no metal was found, neither in the compartments nor at the RPV support. However, with the burst pressure of 1.6 MPa, 4.2% was found at the RPV support, but still very little in the compartments.

The melt trapping device was also tested with a lateral hole (25 mm, 1.1.MPa, water/nitrogen). The dispersed fraction f_d was reduced to 0.10, from 0.36 without the device.

5.3.2. Lateral slot

The amount of water was the same as for lateral holes. The liquid level was 67 mm above the bottom of the calotte and 2 mm above the upper edge of the slot. Two tests with a slot were performed. The vessel pressure curves of the slot and the lateral hole tests are almost identical (not shown) and therefore the gas velocities are the same also (Fig.16).

Due to the higher location of the lower edge of the slot more water remains in the calotte. The difference between post test water level and lower edge, however, is larger (23 versus 20 mm), and therefore, the entrained amount of water (table 2). The reasons are the larger surface area of the water pool in the calotte at this higher position, and the wider flow cross section of the slot versus a round hole. The dispersed liquid fraction, however, is smaller with the slot. In relation to the total amount of water ejected out of the RPV (f_d*), it is 34% for the slot (R02) and 40% for the hole (R03). The dispersed fraction at lower pressure (R01) is small with less than 5%. The correlation to the burst pressure is similar as that for small central holes, i.e. increasing f_d with increasing burst pressure (Fig.21). At lower pressure more water remains in the lower head, because the entrainment is smaller at lower gas velocity, lower density and shorter blowdown time.
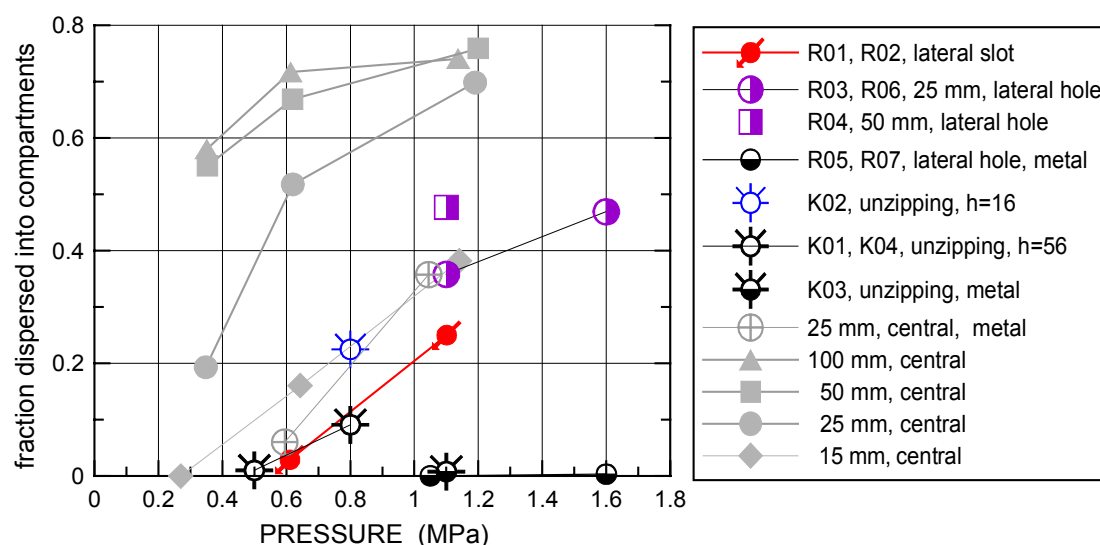

Fig. 21. Dispersed fractions of liquid f_d in test with lateral breaches compared with central holes
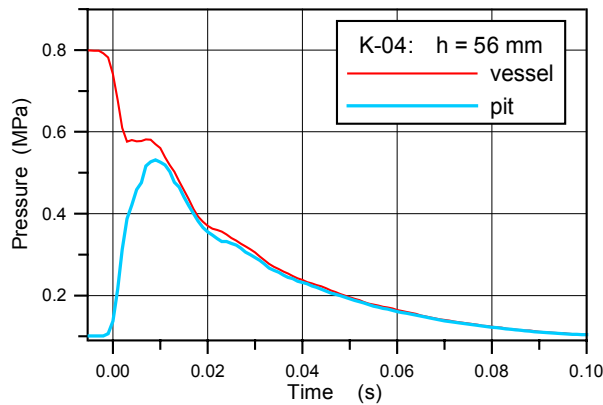
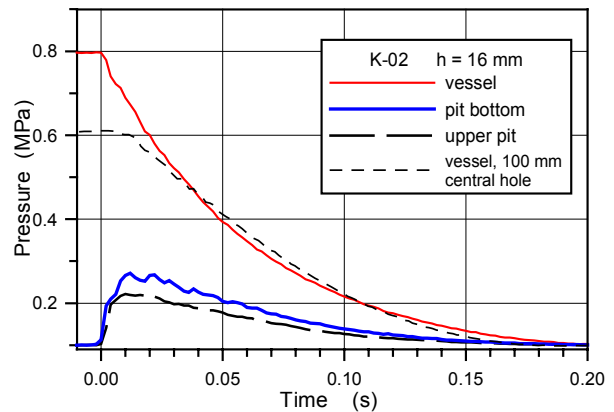**Fig. 22.** Pressures in tests with large drop height of lower head

Fig. 23. Pressures in tests with small drop height of lower head
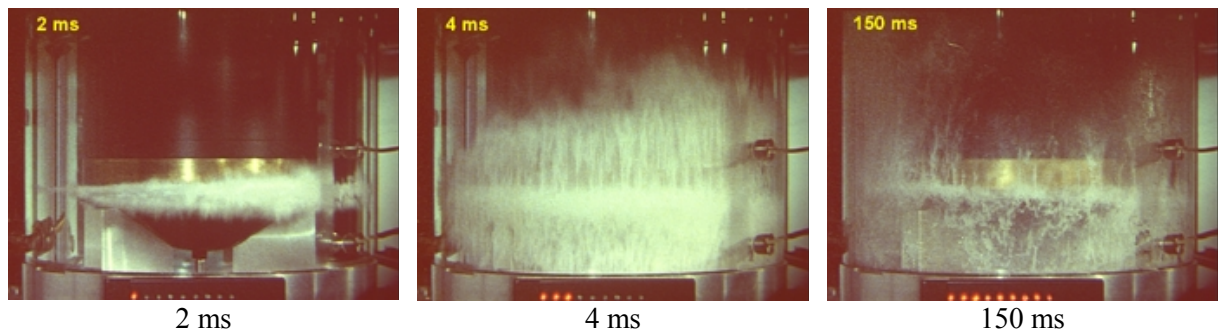

| 2 ms | 4 ms | 150 ms |

Fig. 24. Flow in the reactor pit in test with unzipping of lower head with small drop height (K02)

5.3.3. Unzipping and tilting of the lower head

The amount of water used was 2.1×10^{-3} m³. This scales to 12.3 m³ or approximately 100 t of corium. The water level was 73 mm above the bottom of the calotte and 10 mm above the separating edge. Thus 500 cm³ or 23.5 % of the total mass were above the edge.

Corresponding to the large flow cross section in tests with the high drop height of the calotte, the time for depressurization is extremely short with 0.10 seconds (Fig.22). The other two tests, with the smaller drop height of 16 mm show a similar blowdown curve as tests with the 100-mm central hole (Fig.23).

As for the lateral holes and slots, liquid remains in the lower head after the blowdown. The amount of liquid depends on the tilt angle of the calotte and on the entrainment. The entrainment is larger in tests with the smaller drop height, because of the larger surface area of the remaining water and the longer duration of the blowdown (table 3).

The liquid fraction dispersed out of the cavity is also very small in tests with large drop heights, but somewhat bigger with the smaller drop heights (K04: $f_d = 0.09$, K02: $f_d = 0.23$). With a central 100-mm-hole at an even lower pressure (p = 0.61 MPa) it was $f_d = 0.72$. With the unzipping of the lower head the large break cross section does not lead to high dispersion rates, because the gas does not accelerate the liquid with the lateral break and the entrainment is small because of the extremely short blow down time. Because the entrainment process plays a major role in the case of lateral breaches, the dispersed fraction with metal is very small (K03), even at the higher pressure of 1.1 MPa.

Fig.24 shows the pictures of the flow in the cavity of test K02. The water is ejected through the gap horizontally all around the circumference, with the largest amount at the position opposite to the hinge. The water hits the cavity wall and initially moves upwards and downwards with equal parts. Already at 4 ms a strong upwards directed gas flow can be seen, that makes the water film very thin.

In test K02, after 170 ms the water film moves due to its inertia, the gas flow has ceased. In tests with the larger drop height this occurs already after 80 ms.

6.   CONCLUSIONS

Melt dispersion experiments with different failure modes in the bottom head were carried out in a 1:18 scaled annular cavity design under low pressure conditions. Water and a Bismut-alloy were used as melt simulant material and nitrogen or helium as driving gas.

Several stages take place during the blowdown process at the breach in the lower head: single-phase liquid flow, two-phase flow after the blowthrough and single-phase gas flow, choked and subsonic. The time duration of all these periods depends on the failure mode, the initial pressure and the amount of liquid.

Dispersed melt enters the compartments in two different flow structures:

1. Liquid rivulets or drops resulting from the fragmentation of the liquid film are driven up the cavity walls into the compartments. These drops have larger diameters and lower velocities.

2. Drops are entrained by the gas due to the shearing force existing between gas and liquid film in the annular gap. These drops are carried out of the reactor pit and along the main coolant lines into the compartments by the gas. They have higher velocities and smaller diameters.

With holes at the base of the bottom head the most important parameters governing the dispersion of melt are the hole size and the burst pressure. Practically no liquid remains in the RPV. High dispersal rates can be observed even at pressures below 1 MPa. An almost constant amount of liquid is found at the RPV support, if the liquid reaches this position.

With lateral breaches the liquid height in the lower head relative to the upper and lower edge of the breach is an additional parameter for the dispersion process. In most cases not all the liquid is discharged out of the RPV. Shifting the break from the central position towards the side of the lower head leads to a smaller dispersion of liquid, even if the dispersed fraction is related only to the liquid mass that has been ejected out of the RPV. The main effect is probably the circumferential component of the velocity in the cavity. If the initial liquid level is above the upper edge, the blowdown starts with the single-phase liquid discharge, driven by the pressure difference between vessel and cavity, as for central holes. However, the gas blowthrough occurs earlier than with central holes. In the subsequent stage the liquid is carried out of the lower head by entrainment. The gas velocity, the density ratio of gas and liquid, the surface area of the liquid pool, and the duration of the blowdown govern this entrainment process. Therefore, the entrained liquid fraction can be higher with a small breach than with a large one, because the blowdown time is longer but the maximum velocity may be the same. Also the fraction of melt dispersed out of the reactor pit may be larger with smaller lateral breaches than with very large ones.

The application of the results from lateral failures to the reactor scale is more difficult than in the case of central holes. Investigations of similarity for the process of entrainment within the lower head have not been undertaken yet. Zero-dimensional codes need correlations for the lateral breaches that are not available due to the limited data basis. CFD-codes have not been applied yet in three dimensions, but it is planned to do so. As for the time being, we can make the cautious statement, that taking the known similarity correlations, the results from the liquid metal tests represent the lower bound for the dispersed melt fractions, however, they are probably closer to the expected values than the results from the water tests, that represent the upper bound. So, significantly less dispersion of melt can be expected for lateral breaches at pressures below 2 MPa, probably less than 10%. If higher dispersion occurs, due to higher

pressure at failure, simple devices to mitigate the dispersion out of the cavity may be feasible. For the investigation of thermal and chemical effects experiments with alumina-iron melt and steam will be performed in a similar geometry.

References

1. Nucl. Eng. Des., 164, 1996 (Topical Issue on DCH).

2. Bertodano, M. L. de, A. Becker, A. Sharon, R. Schnider, DCH Dispersal and entrainment experiment in a scaled annular cavity, Nucl. Engng. Des.,164, 271-285, 1996.

3. Blanchat, T.K., M. Pilch, and M.D. Allen, Experiments to Investigate Direct Containment Heating Phenomena with Scaled Models of the Calvert Cliffs Nuclear Power Plant, NUREG/CR-6469, SAND96-2289, Sandia National Laboratories, Albuquerque, N.M., 1997.

4. Blanchat, T.K., M.M. Pilch, R.Y. Lee, L. Meyer, and M. Petit, Direct Containment Heating Experiments at Low Reactor Coolant System Pressure in the Surtsey Test Facility, NUREG/CR-5746, SAND99-1634, Sandia National Laboratories, Albuquerque, N.M., 1999.

5. Kim, S.B, R.J. Park, H.D. Kim, Chevall and M.Petit, Reactor Cavity Debris Dispersal Experiment with Simulant at Intermediate System Pressure, Proc. Seminar on Containment of Nuclear Reactors, Post Conference Seminar to the 15th SMiRT, Seoul, Korea, August 23-24, 1999.

6. Jacobs, G., L. Meyer, Planned melt dispersal experiments in a scaled cavity, SMiRT14 Post Conference Seminar on Containment of Nuclear Reactors, CEA Sacley, France, August 25-26, 1997.

7. Wilhelm, D., Transient Code Models for Low Pressure Corium Dispersion, OECD Workshop on Ex-Vessel Debris Coolability, Karlsruhe, Germany, 15-18 November 1999.

8. Zuber, N. et al., An integrated structure and scaling methodology for severe accident technical issue resolution: Development of methodology, Nuclear Engineering Design, 186, 1-21, 1998; and NUREG/CR-5809 EGG-2659, 1991.

9. Ishii, M., H.G. No and G. Zhang, Stepwise integral scaling method and its application to severe accident phenomena, NUREG/GR-0009, 1993.

10. Tutu, N.K., T. Ginsberg, C. Finrock et al., Debris Dispersal from Reactor Cavities during High-Pressure Melt Ejection Accident Scenarios, BNL, NUREG/CR-5146, 1988.

11. Pilch, M.M., A two-cell equilibrium model for predicting direct containment heating, Nuclear Engineering Design, 164, 61-94, 1996.

12. Chu, T.Y., M. Pilch, J.H. Bentz and A.Behbahani, Experimental Investigation of Creep Behavior of Reactor Vessel Lower Head, OECD/CSNI Workshop on In-Vessel Core Debris Retention and Coolability, Garching, Germany, 3-6 March, 1998.

13. Meyer, L., G. Jacobs, D. Wilhelm, M. Gargallo, T. K. Blanchat, Experiments on Corium Dispersion after Lower Head Failure at Moderate Pressure, Post Conf. Seminar on Containment of Nuclear Reactors, Seoul, Korea, August 23-24. 1999.

14. Meyer, L., Experiments to Investigate the Low Pressure Corium Dispersion in EPR Geometry, Proc. OECD Workshop on Ex-Vessel Debris Coolability, Karlsruhe, Germany, 15-18 November 1999, Ed. H. Alsmeyer, Forschungszentrum Karlsruhe, FZKA 6475, 2000.

15. Pilch, M.M., R.O.Griffith, Gas Blowthrough and flow quality correlations for use in the analysis of high pressure melt ejection (HPME) events, SANDIA Report, SAND91-2322, UC-523, Sandia National Laboratories, June 1992.

16. Meyer, L., M. Gargallo, M. Greulich, M. Kirsthaler, M. Schwall, G. Wörner, E. Wachter, "Low Pressure Corium Dispersion Experiments in the DISCO-C Tests Facility with Cold Simulant Fluids", FZK-Report 6591, Forschungszentrum Karlsruhe, to be published in 2001.